Thyrocyte cell survival and adaptation to chronic endoplasmic reticulum stress due to misfolded thyroglobulin

Received for publication, January 14, 2020, and in revised form, March 29, 2020 Published, Papers in Press, April 2, 2020, DOI 10.1074/jbc.RA120.012656

Yoshiaki Morishita[‡§1], Omer Kabil[‡1], Kelly Z. Young[‡], Aaron P. Kellogg[‡], Amy Chang[¶], and Peter Arvan[‡2]

From the [‡]The Division of Metabolism, Endocrinology & Diabetes, University of Michigan Medical Center, Ann Arbor, Michigan 48105, [§]Division of Diabetes, Department of Internal Medicine, Aichi Medical University, Aichi 480-1195 Japan, and [¶]Department of Molecular, Cellular and Developmental Biology, University of Michigan, Ann Arbor, Michigan 48109

Edited by Ronald C. Wek

The large secretory glycoprotein thyroglobulin is the primary translation product of thyroid follicular cells. This difficult-to-fold protein is susceptible to structural alterations that disable export of the misfolded thyroglobulin from the endoplasmic reticulum (ER), which is a known cause of congenital hypothyroidism characterized by severe chronic thyrocyte ER stress. Nevertheless, individuals with this disease commonly grow a goiter, indicating thyroid cell survival and adaptation. To model these processes, here we continuously exposed rat PCCL3 thyrocytes to tunicamycin, which causes a significant degree of ER stress that is specifically attributable to thyroglobulin misfolding. We found that, in response, PCCL3 cells down-regulate expression of the "tunicamycin transporter" (major facilitator superfamily domain containing-2A, *Mfsd2a*). Following CRISPR/Cas9-mediated *Mfsd2a* deletion, PCCL3 cells could no longer escape the chronic effects of high-dose tunicamycin, as demonstrated by persistent accumulation of unglycosylated thyroglobulin; nevertheless, these thyrocytes survived and grew. A proteomic analysis of these cells adapted to chronic ER protein misfolding revealed many hundreds of up-regulated proteins, indicating stimulation of ER chaperones, oxidoreductases, stress responses, and lipid biosynthesis pathways. Further, we noted increased phospho–AMP-kinase, suggesting up-regulated AMP-kinase activity, and decreased phospho–S6-kinase and protein translation, suggesting decreased mTOR activity. These changes are consistent with conserved cell survival/adaptation pathways. We also observed a less-differentiated thyrocyte phenotype with decreased PAX8, FOXE1, and TPO protein levels, along with decreased thyroglobulin mRNA levels. In summary, we have developed a model of thyrocyte survival and growth during chronic continuous ER stress that recapitulates features of congenital hypothyroid goiter caused by mutant thyroglobulin.

This work was supported by NIDDK, National Institutes of Health Grant R01 DK40344 (to P. A.); NIGMS, National Institutes of Health MSTP training Grant T32 GM007863 (to K. Z. Y.); and NIA, National Institutes of Health Grant R21 AG058862 (to A. C.). This work was also supported by the University of Michigan Protein Folding Diseases Initiative (to A. C. and P. A.). The authors declare that they have no conflicts of interest with the contents of this article. The content is solely the responsibility of the authors and does not necessarily represent the official views of the National Institutes of Health.

This article contains Figs. S1–S4 and Tables S1 and S2.

[1] These authors contributed equally to this work.

[2] To whom correspondence should be addressed. Tel.: 734-936-5505; E-mail: parvan@umich.edu.

Protein misfolding in the endoplasmic reticulum (ER)[3] is continuously monitored through ER stress sensing and signaling pathways. Activation of IRE1, PERK, and ATF6, collectively, transmits responses that lead to inhibition of global protein synthesis while increasing ER chaperones and protein folding factors, accompanied by increased ER-associated and autophagic degradation of misfolded proteins (1). However, under conditions of chronic continuous ER stress (2), cell death pathways can become activated (3), although cell proliferation can become limited (4). When cell proliferation is insufficient to compensate for cell loss, functional tissue mass may decline, as has been postulated in the case of pancreatic β-cell failure in several forms of diabetes (5). Conversely, when the stimulation of cell growth outpaces cell loss, there is actual net tissue expansion, as in the development of thyroid goiter in several forms of thyroid dyshormonogenesis (6). ER stress–mediated disease may take months or years to become clinically apparent, which poses a significant challenge when trying to correlate experimental ER stress studies that are often conducted on a short time scale (7).

Thyroglobulin (Tg) misfolding as a cause of congenital hypothyroidism represents a valuable system in which to explore cell death or survival in the face of chronic ER stress. The defect within the ER is severe (8), yet (unlike deleterious effects of chronic hyperglycemia on pancreatic β-cells) hypothyroidism itself is nontoxic to thyrocytes. *TG* is the most highly expressed thyroid gene. The Tg protein comprises >50% of all thyroidal protein, and its export through the secretory pathway is required for thyroid hormone synthesis (9). Most pathogenic Tg mutants are misfolded and entrapped in the ER, causing chronic ER stress with hypothyroidism (10), which triggers a well-understood endocrine feedback loop that increases circulating thyrotropin (TSH) that is linked to thyrocyte proliferation, promoting thyroid gland growth in humans and animal models. Yet, many studies suggest that cell death with loss of tissue mass is the expected consequence of chronic unremitting ER stress (3, 11). Until now there have been few or no studies examining how thyrocytes with massive misfolding of Tg in the ER can avoid loss of thyroid cell mass.

In this report we have developed a cell culture model of PCCL3 thyrocytes surviving and growing in the face of chronic continuous ER stress with accumulation of misfolded Tg.

[3] The abbreviations used are: ER, endoplasmic reticulum; Tg, thyroglobulin; TSH, thyrotropin; TUN, tunicamycin; ROS, reactive oxygen species; phospho-AMPK, phosphorylated AMP kinase.

Importantly, TSH is not a variable in our cell culture studies and plays no direct role in the adaptive response to chronic ER stress in this model. With this in mind, we find that PCCL3 cells surviving chronic unremitting ER stress have fairly dramatic changes in the whole cell proteome, suggesting persistently up-regulated ER stress responses including the pro-apoptotic transcription factor, CHOP, plus ER lipid biosynthetic activity, activated AMP-kinase, increased autophagy, and a suggestion of down-regulated mTOR signaling and global protein synthesis, and subtle signs of thyrocyte de-differentiation accompanying significantly decreased *TG* mRNA levels. With these global changes, remarkably, thyrocytes continue to grow both in our cell culture model and, we show, *in vivo* as well.

Results

Thyrocytes survive and grow in the presence of chronic continuous ER stress

Patients suffering from congenital hypothyroidism with defective thyroglobulin often develop thyroid gland overgrowth (goiter) (12). This has also been found in some animal models of the disease (13). The homozygous $TG^{cog/cog}$ mouse encodes expression of misfolded Tg that is defective for export from the ER, triggering chronic continuous ER stress in the thyroid gland from neonatal life through adulthood (14). Despite this, we confirmed ongoing thyroid follicular epithelial cell (thyrocyte) proliferation (as measured by Ki67 immunocytochemistry) (Fig. S1). Thus, thyrocytes can indeed survive and adapt to chronic, continuous ER stress. We therefore wondered if it was possible to develop a simple cell culture model of thyrocyte adaptation to chronic ER stress with thyroglobulin misfolding.

Thyrocytes are dedicated to the biosynthesis of the Tg glycoprotein (15), which ordinarily accounts for more than half of all of the protein of the thyroid gland (16). With this in mind, we examined ER stress response upon CRISPR/Cas9-mediated disruption of *TG* in PCCL3 thyrocyte clones with undetectable Tg synthesis (*TG*-KO) (Fig. 1, *A* and *B*). *TG*-KO clones showed a ≥30% decrease in basal levels of BiP mRNA (Fig. 1*C*); additionally, tunicamycin (TUN) treatment induced BiP and CHOP mRNA by only ∼half that obtained from treatment of control thyrocytes (Fig. 1, *D* and *E*). After 48 h with 25 ng/ml TUN treatment of control PCCL3 cells (that express Tg protein), misfolded Tg could be visually seen to accumulate in the ER, accompanied by stress-induced up-regulation of ER resident proteins (Fig. 1, *G* and *H*). Even with an acute challenge of 100 ng/ml TUN, a majority of thyrocytes survived at 48 h (*i.e.* 39% dead) with significantly greater survival in *TG*-KO cells (Fig. 1*F*). Altogether, these data suggest that expression of the endogenous Tg glycoprotein contributes significantly to basal ER stress in thyrocytes with an even greater contribution to ER stress induced by TUN treatment.

Development of a cell culture model of chronic continuous ER stress

Based on the foregoing results, we sought to explore the behavior of chronically ER-stressed PCCL3 cells maintained in the continuous presence of TUN, with persistent Tg misfolding. After a 7-d exposure to 25 ng/ml TUN, ER stress was still apparent as detected by increased phospho-eIF2α; however, by ∼2 months of continuous culture, the increased level of phospho-eIF2α significantly abated (Fig. 2*A*). To determine whether this represents adaptation to chronic ER stress or escape from the effects of TUN, we followed the glycosylation of endogenous Tg throughout the experimental time course. After 7 d of TUN, >90% of intracellular Tg was unglycosylated (Fig. 2*B*, *upper panel*), and essentially no Tg was secreted into the medium (*lower panel*). However, by 2 weeks after initiation of TUN treatment we noted the beginning of a return of Tg secretion, and by ∼ 1 month of treatment there was a notable decline in intracellular unglycosylated Tg accompanied by an increase of Tg glycosylation and secretion (Fig. 2*B*). Recognizing this, we conducted experiments in which cells escaping the effects of low-dose TUN were challenged with successively higher doses. After each increment of TUN concentration, PCCL3 cells accumulated unglycosylated Tg intracellularly and secreted almost no Tg into the media, but in each case, thyrocytes eventually lost the inhibition of *N*-glycosylation by TUN (Fig. 2*C*). With each dose increase, thyrocytes initially slowed their growth rate but then returned to the same passage frequency as that of control cells. Thyrocytes successively exposed to increasing doses of TUN developed obvious swelling of the ER, as judged by EM (Fig. 2*D*). Given the obvious escape from inhibition of *N*-glycosylation, we examined expression of the lysophosphatidylcholine/docosahexaenoate transporter *Mfsd2a*, which is known to encode the primary plasmalemmal transport mechanism for TUN (17, 18). Indeed, PCCL3 cells that had been slowly adapted to increasing doses of TUN eventually suppressed *Mfsd2a* mRNA expression >500-fold (Fig. 2*E*). Compatible with successive escape from inhibition of *N*-glycosylation by TUN, we noted that with each stepwise dose increment, ER stress response was activated followed by subsequent recovery, as measured by a restoration of BiP and CHOP mRNA toward initial, control levels (Fig. 2*F*). However, we noted that at the highest dose of TUN achieved by stepwise increment (300 ng/ml), the cells' defect in *N*-glycosylation of Tg persisted for the duration of our experiments, indicating that it is possible with high dose TUN to inhibit *N*-glycosylation despite a profound loss of *Mfsd2a* expression. At this highest dose, similar to the lower doses, after an initial slowing of growth rate the cells resumed a passage frequency identical to that of untreated control cells (although at this point, the cells had been growing in sequential culture for more than 1 year).

Because PCCL3 cells repeatedly escaped effects of sequential TUN until 1 year in culture by down-regulating *Mfsd2a* expression, we reasoned that cells bearing genetic deficiency of *Mfsd2a* (while being resistant to low-dose TUN) would be immediately sensitive to high-dose TUN yet, under these conditions, would be defective for escape from the inhibition of *N*-glycosylation. With this in mind, we used CRISPR/Cas9-mediated disruption of *Mfsd2a* in PCCL3 thyrocyte clones with confirmation of frameshift (*Mfsd2a*-KO). Two PCCL3 clones exhibited identical phenotypes (*e.g.* Fig. S3); most of the experiments shown in this study used clone A5.

When challenged with a range of TUN doses for 24 h, control PCCL3 cells already showed a dramatic activation of ER stress response at a dose of 0.1 μg/ml TUN (as measured by the ratio

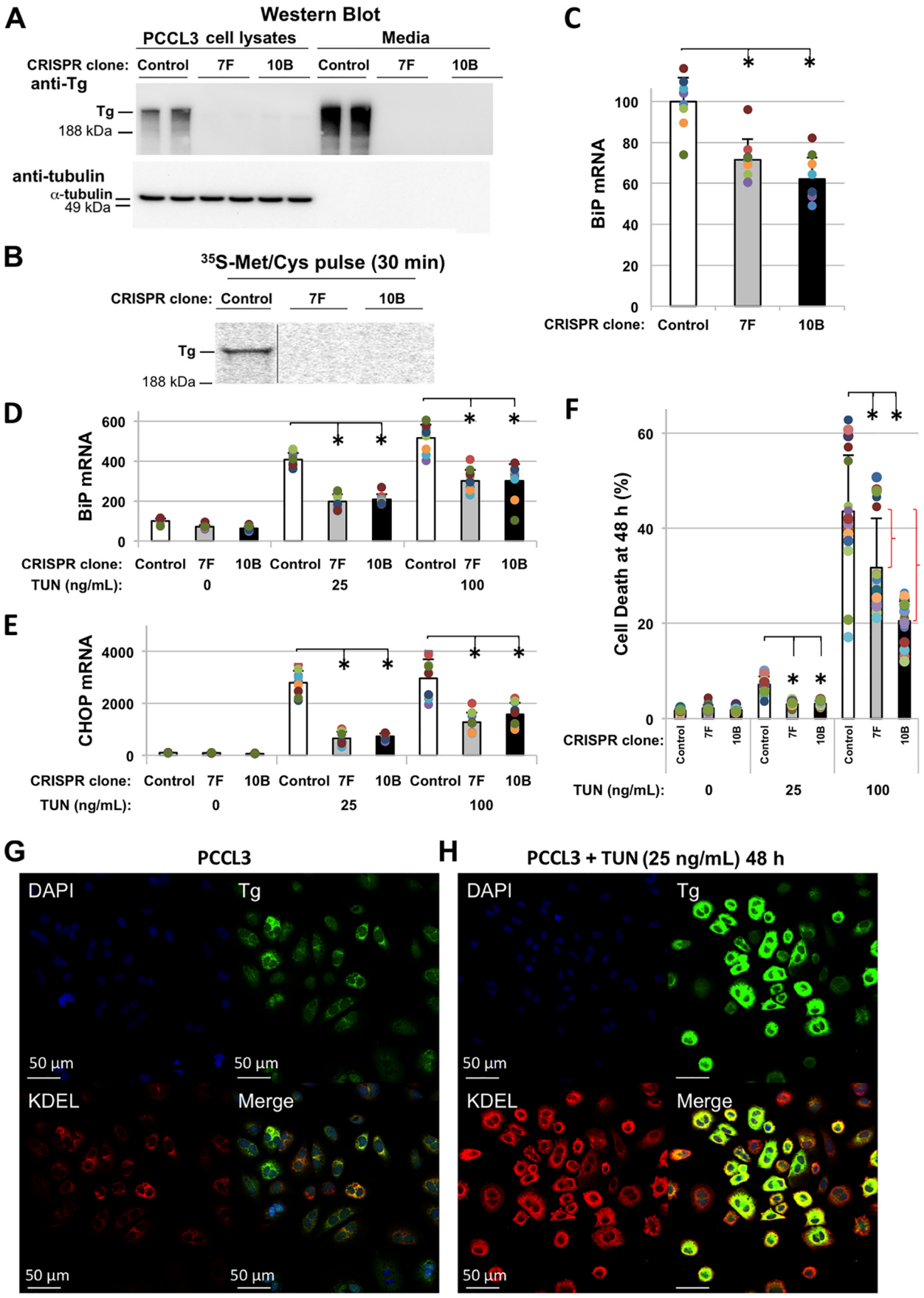
A
Western Blot
PCCL3 cell lysates
Media
CRISPR clone: Control 7F 10B Control 7F 10B
anti-Tg
Tg
188 kDa
anti-tubulin
α-tubulin
49 kDa
B
35S-Met/Cys pulse (30 min)
CRISPR clone: Control 7F 10B
Tg
188 kDa
C
BiP mRNA
CRISPR clone: Control 7F 10B
D
BiP mRNA
CRISPR clone: Control 7F 10B Control 7F 10B Control 7F 10B
TUN (ng/mL): 0 25 100
E
CHOP mRNA
CRISPR clone: Control 7F 10B Control 7F 10B Control 7F 10B
TUN (ng/mL): 0 25 100
F
Cell Death at 48 h (%)
CRISPR clone: Control 7F 10B Control 7F 10B Control 7F 10B
TUN (ng/mL): 0 25 100
G
PCCL3
DAPI
Tg
KDEL
Merge
50 µm
H
PCCL3 + TUN (25 ng/mL) 48 h
DAPI
Tg
KDEL
Merge
50 µm

of spliced to unspliced XBP1 that depends upon Ire1) (19), whereas homozygous *Mfsd2a*-KO cells yielded similar ER stress only after an order of magnitude increase in TUN concentration (Fig. 3*A*, *left*). Consistent with these findings, control PCCL3 cells exhibited a similar TUN dose sensitivity for increased eIF2α phosphorylation (suggestive of PERK activation) (20), as well an increase in the steady-state levels of BiP and CHOP (Fig. 3*B*), two well-recognized targets of the ER stress response (21). Further, whereas low-dose TUN nearly completely blocked Tg secretion from control PCCL3 cells, a comparable block of Tg secretion from *Mfsd2a*-KO cells also required an order of magnitude higher TUN concentration (Fig. 3*C*, *left*). Similarly, although thyrocytes must generate ROS (in the form of H_2O_2) for thyroid hormone synthesis, *Mfsd2a*-KO cells exhibited less TUN-induced ROS as judged either by dihydroethidium fluorescence imaging (Fig. S2) or as quantified by dihydrorhodamine 123 fluorescence (Fig. 3*D*). The *Mfsd2a*-KO cells required more than or equal to an order of magnitude increase in TUN dose to trigger a comparable degree of acute ER stress–induced cell death (Fig. 3*E* and Fig. S3). By contrast, sensitivity of both sets of thyrocytes to another ER stress inducer (thapsigargin, 250 nM, 24 h) were comparable as judged by XBP1 splicing (Fig. 3*A*, *right*), with a similar inhibition of Tg secretion (sampled at 24–72 h) (Fig. 3*C*, *right*). Thus, *Mfsd2a*-KO thyrocytes are resistant to low-dose TUN but they are not defective in sensitivity to ER stress.

Thyrocytes that survive and adapt to chronic, continuous ER stress

As noted above, we predicted that *Mfsd2a*-KO thyrocytes would be relatively incapable of escape from inhibition of *N*-glycosylation in the persistent presence of high-dose TUN. Indeed, even after a continuous 4-month exposure to TUN at a dose of 1500 ng/ml, Tg contained within the *Mfsd2a*-KO cells remained unglycosylated (Fig. 4*A*, *U*) and could not be secreted into the medium (Fig. S4). Over this lengthy period of continuous culture, BiP mRNA remained elevated (Fig. 4*B*), accompanied by an increase of KDEL-containing ER-resident proteins including BiP, GRP94, and others (as measured by Western blotting (Fig. 4*C*). Moreover, *Mfsd2a*-KO thyrocytes grown in the continuous presence of 1500 ng/ml TUN exhibited persistently increased phospho-eIF2α (not shown) accompanied by increased CHOP levels (Fig. 4*C*). Despite this, the chronic continuously ER-stressed thyrocytes exhibited an overall cell growth rate that was not significantly different from that of the same cells grown in the complete absence of TUN (Fig. 4*D*).

These adapted thyrocytes reproducibly exhibited an increase of phospho-AMP-kinase (our antibody recognizes phospho–Thr-172 of the AMPK α-subunit). To evaluate if this represents part of the physiological adaptive response of thyrocytes to chronic continuous ER stress, we analyzed thyroid gland tissue of TG^{cog}/TG^{cog} mice (homozygously expressing the misfolded mutant Tg-L2263P) and indeed observed very similar behavior (Fig. 5*B*). Thus, an increase in the pro-apoptotic transcription factor CHOP in the face of chronic continuous ER stress does not preclude extensive overall cell proliferation (Fig. 4*D* and Fig. S1) which underlies goiter development (22). Moreover, we considered the possibility that the activation of AMPK helps to limit ER stress–mediated cell death; indeed, we observed that addition of the AMPK chemical activator 769662 significantly decreased cell death of "virgin PCCL3" thyrocytes in response to an acute ER stress challenge with high-dose TUN (Fig. 5*C*). Accompanying the activation of AMPK was a notable decrease in the extent of phosphorylation of ribosomal S6-kinase (Fig. 5*D*), which is a known downstream target of the mTOR signaling cascade and a contributing regulator of protein synthesis capacity (23). Remarkably, the growth rate of the chronically adapted thyrocytes was essentially normal (Fig. 4*D*), and the cells simultaneously maintained a lower overall protein synthesis rate (established by amino acid radiolabeling, Fig. 5*E*).

We performed a comprehensive proteomic analysis of up- and down-regulated proteins in three independent replicate cultures of chronically ER-stressed thyrocytes. Remarkably, there was very low variability between the replicates, indicating low biological heterogeneity plus low variance in sample preparation and protein separation, leading to excellent quantitative correlation between samples. The majority of detected changes in protein content represented proteins up-regulated in chronically ER-stressed cells (Table S1). From software-enabled Gene Ontology analysis proteins involved in signaling pathways, gene regulatory pathways, and metabolic pathways, we were able to deduce the major up-regulated biological pathways in the *Mfsd2a*-KO thyrocytes chronically stressed by continuous high-dose TUN exposure (Fig. 6). Of more than 4000 total protein identifications, <10% showed a significant increase in concentration, with a tendency to fall into pathways linked to tRNA synthetase activity (coupled to ATF4 function), nucleotide/ATP binding (coupled to chaperone function), and ER homeostasis (Fig. 6 and Table S2). Only a minority of the highly up-regulated pathways in the continuous TUN-treated cells were plausibly correlated to functional inhibition of *N*-glycosylation, focused primarily on increased basal lamina/extracellular matrix proteins required for cell-cell or cell-matrix attachment. Additionally, other novel pathways were up-regulated in cells adapted to these chronic stress conditions (Fig. 6).

Of the fewer down-regulated proteins, we noted subtle signs of thyrocyte de-differentiation, including a decrease of thyroid transcription factors FOXE1 and PAX8, as well as decreased thyroid peroxidase (TPO) protein expression (Fig. 7*A*). Because misfolded Tg accumulates intracellularly (within the ER) (Figs. 4*A* and 5*A* and Fig. S4), its intracellular protein level is not a good means to look for altered protein expression/de-differen-

Figure 1. Expression of Tg protein contributes importantly to endogenous and tunicamycin-induced ER stress. *A*, anti-Tg Western blotting of WT PCCL3 thyrocytes and 24-h conditioned (serum-free) media; similarly, from two *TG*-KO clones. *B*, newly synthesized Tg in cells from *A*. *C* and *D*, basal BiP mRNA levels (*C*) and after 48 h of tunicamycin (TUN) in control (*open*) and two *TG*-KO clones (*D*): 7F (*gray*) and 10B (*black*). *E*, CHOP mRNA as in *D*; *error bars* represent mean ± S.D. (three independent experiments, nine biological replicates), *, $p < 0.05$ *versus* control. *F*, cell death upon TUN (48 h) treatment; *error bars* represent mean ± S.D. (five independent experiments), *, $p < 0.05$ *versus* control. *Red brackets* indicate the difference in cell death specifically attributable to expression of *TG*. *G* and *H*, immunofluorescence: anti-Tg (*green*), anti-KDEL (*red*).

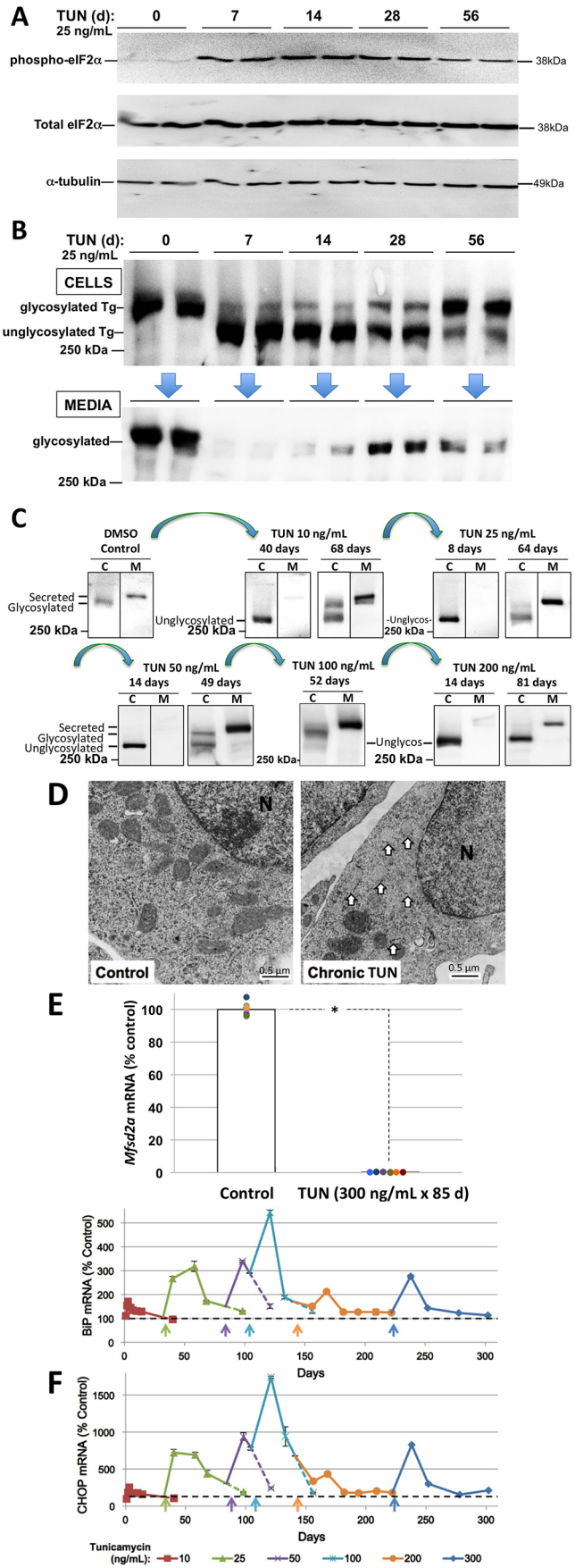

Figure 2. PCCL3 thyrocytes escape from TUN. *A*, phospho-eIF2α (and total eIF2α and α-tubulin loading controls) in PCCL3 cells treated continuously with TUN (25 ng/ml) and lysed at different time points for up to 56 days of culture. *B*, Tg protein recovered in cells and 24-h conditioned (serum-free) media collected from the same cells shown in *panel A*. *C*, PCCL3 cells exposed continuously to sequentially higher and higher doses of TUN. At each dose, the cells begin by being sensitive to inhibition of Tg glycosylation, but at each dose, after a period of weeks, the thyrocytes have escaped as demonstrated by the presence of glycosylated Tg in the cells (*C*) and/or medium (*M*). *D*, transmission EM of control PCCL3 cells and those from the end of the experiment in *panel C*. *E*, PCCL3 cells advanced beyond *panel C*, to a TUN dose of 300 ng/ml for a further 85 d of continuous culture, at which time total RNA was isolated and *Mfsd2a* mRNA levels (normalized to 18S RNA) were quantified. *Error bars* represent mean ± S.D. (with statistical significance) from three independent experiments in which each sample had three biological replicates (nine total samples for each condition). *F*, qRT-PCR analysis of BiP (*above*) and CHOP (*below*) mRNA in PCCL3 cells grown continuously for nearly a year with stepwise increased TUN doses (10, 25, 50, 100, 200, and 300 ng/ml, indicated in distinct colors), normalized to mRNA levels in control cells grown in parallel with vehicle alone; *error bars* represent mean ± S.D.; $n = 3$ at each time point.

tiation. However, at the mRNA level in chronically ER-stressed thyrocytes, *TG* expression was notably inhibited (Fig. 7*B*), which might reflect diminished transcription (24, 25) or ER stress–mediated degradation of *TG* mRNA (RIDD) (26). Regardless of mechanism, diminished *TG* mRNA levels accompany the physiological adaptive response to chronic continuous ER stress as it is also noted in the thyroid glands of TG^{cog}/TG^{cog} mice (Fig. 7*C*).

Discussion

We have cited the $TG^{cog/cog}$ mouse as a physiological model of chronic continuous ER stress (14), but this is but one of a myriad of diseases in which misfolded proteins continue to be synthesized and accumulate in the ER for months or years of life (27). Homozygous patients synthesizing the hepatic Z-variant of α1-antitrypsin from birth do not develop cirrhotic liver failure until around age 50, indicating decades during which a population of surviving hepatocytes must contend with the misfolding-prone mutant protein in the ER (28).

To the best of our knowledge, there have really been no cell culture models of chronic continuous ER stress in mammalian cells, and despite valiant attempts to emulate disease-related adaptation by treatment of cells or tissues with acute pharmacological ER stress agents for up to a few days (29), these attempts fail to emulate the full spectrum of adaptive responses that take weeks (or longer) to develop (7). Whereas mild acute ER stress has been reported to be pro-proliferative (30), chronic continuous severe ER stress can block such proliferation (31, 32), and conventional wisdom has suggested that in such cases, cell death prevails (33, 34). However, this does not account for the reality that some tissues bearing such stress can and do survive, despite the pathology, for months or years. Nowhere is this more remarkable than in the thyroid gland, in which hypothyroid patients bearing homozygous *TG* mutations not only continue to synthesize the mutant protein, but they also develop goiter, thyrocyte hyperplasia leading to actual thyroid gland enlargement (35), which is also seen in the $TG^{cog/cog}$ mouse model (Fig. S1).

In this report, we have developed a continuous growing line of thyrocytes that adapt to the continuous production and ER misfolding of the large Tg glycoprotein. Our initial studies demonstrated that the ongoing production of Tg contributes importantly to both the basal ER stress set point in thyrocytes,

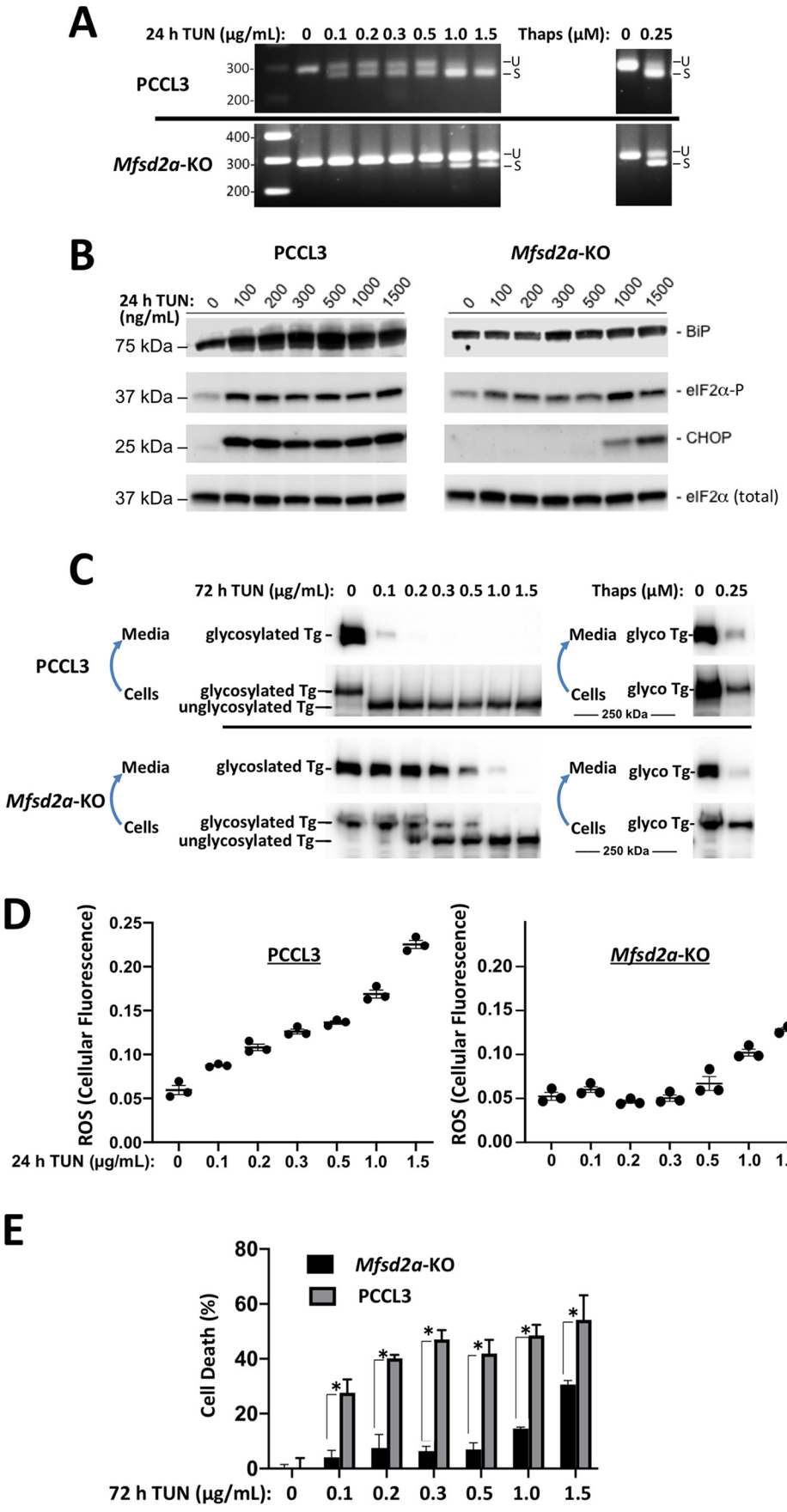
A
24 h TUN (μg/mL): 0 0.1 0.2 0.3 0.5 1.0 1.5
Thaps (μM): 0 0.25
PCCL3
Mfsd2a-KO
300-
200-
400-
U
S
B
PCCL3
Mfsd2a-KO
24 h TUN: (ng/mL)
0 100 200 300 500 1000 1500
75 kDa –
37 kDa –
25 kDa –
37 kDa –
- BiP
- eIF2α-P
- CHOP
- eIF2α (total)
C
72 h TUN (μg/mL): 0 0.1 0.2 0.3 0.5 1.0 1.5
Thaps (μM): 0 0.25
PCCL3
Mfsd2a-KO
Media
Cells
glycosylated Tg -
glycosylated Tg—
unglycosylated Tg—
glycoslated Tg-
glyco Tg-
250 kDa
D
PCCL3
Mfsd2a-KO
ROS (Cellular Fluorescence)
0.25
0.20
0.15
0.10
0.05
0.00
24 h TUN (μg/mL): 0 0.1 0.2 0.3 0.5 1.0 1.5
E
Mfsd2a-KO
PCCL3
Cell Death (%)
80
60
40
20
0
*
72 h TUN (μg/mL): 0 0.1 0.2 0.3 0.5 1.0 1.5

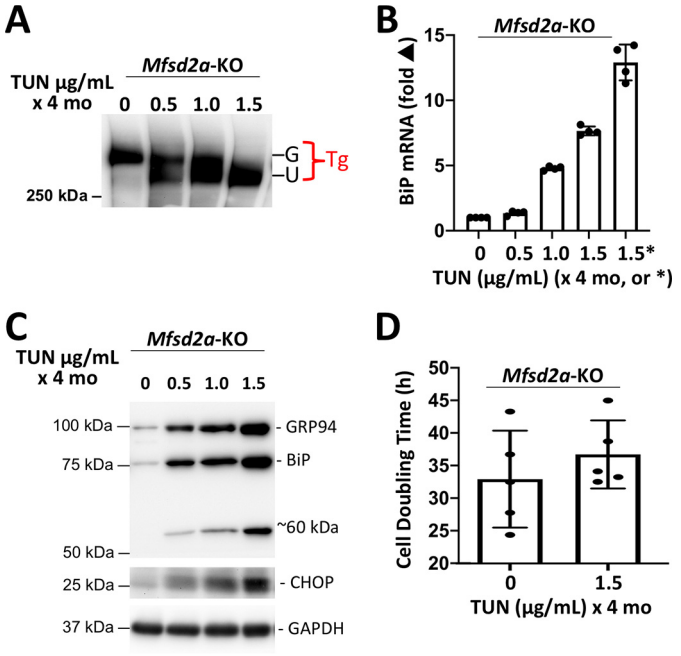

Figure 4. Chronic severe ER stress in *Mfsd2a*-KO thyrocytes cultured in the continuous presence of high-dose TUN (four months). *A*, immunoblotting of intracellular Tg. *G*: glycosylated, *U*: unglycosylated. *B*, BiP mRNA levels in the cells shown in *panel A*, and also in "virgin cells" acutely treated with high-dose TUN for 24 h (*asterisk*). *C*, immunoblots with anti-KDEL (*upper panel*, the positions of GRP94 and BiP are noted; the band at the ~60 kDa position may be PDI, ERp57, or calreticulin) and CHOP (GAPDH is a loading control). *D*, cell doubling time in *Mfs32a*-KO cells under control growth conditions or after the chronic continuous presence of high-dose TUN.

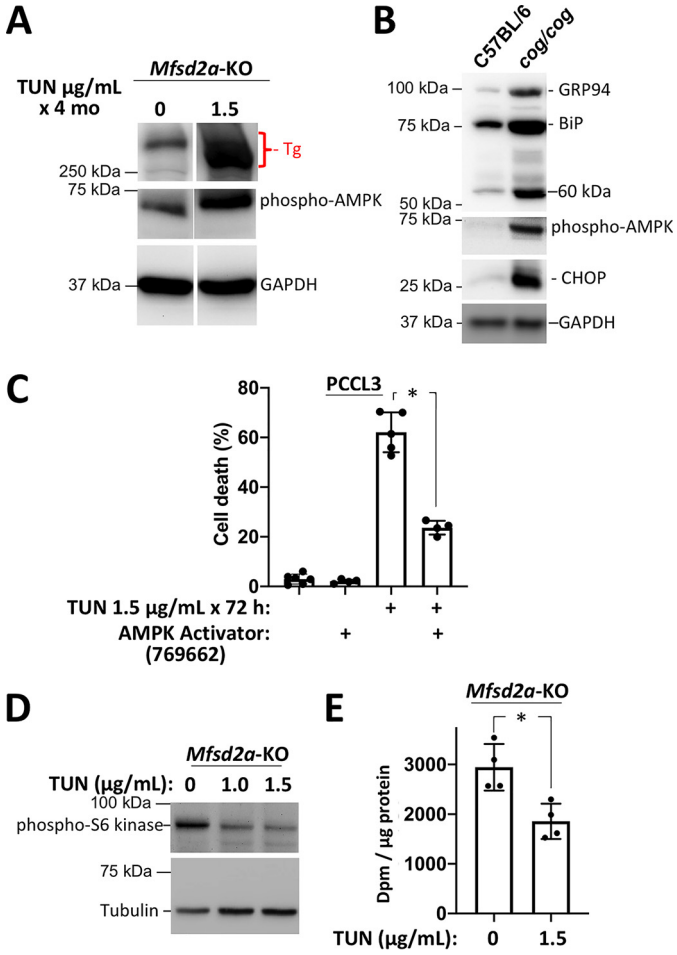

Figure 5. Survival and adaptation to ER stress in *Mfsd2a*-KO thyrocytes. *A*, phospho-AMPK (α-subunit Thr-172; a concurrent Tg immunoblot confirms accumulation of unglycosylated intracellular Tg; GAPDH is a loading control). *B*, WT control mouse (C57BL/6) and $TG^{cog/cog}$ thyroid tissue, immunoblotted with anti-KDEL (*upper panel*, the positions of GRP94 and BiP are noted; the band at the ~60 kDa position may be PDI, ERp57, or calreticulin), CHOP (*bottom panel*), and anti–phospho-AMPK (a subunit Thr-172). GAPDH is a loading control. *C*, control PCCL3 thyrocytes were acutely challenged with (or without) high-dose TUN in the presence or absence of the AMP-kinase (AMPK) activator (A-769662, 200 μM); cell death at 48 h was measured using the Cyto-Tox Glo kit. *D*, immunoblot of phospho–S6-kinase (tubulin is a loading control) in *Mfsd2a*-KO thyrocytes under control growth conditions or after the chronic continuous presence of TUN (doses shown). *E*, overall protein translation rate in *Mfsd2a*-KO thyrocytes under control growth conditions, or after the chronic continuous presence of high-dose TUN, as measured by ^{35}S-amino acid incorporation into TCA-precipitable proteins per hour per microgram protein.

and also to the acute ER stress response to a low-dose TUN challenge (Fig. 1). Indeed, such a challenge blocks Tg glycosylation, triggers phosphorylation of eIF2α, and stimulates the expression of established downstream targets of the ER stress response (Fig. 2). However, although these features were apparent for ~2-weeks in culture they could not be maintained thereafter, even upon our considerable effort to overpower the system with ever-increasing doses of TUN (Fig. 2*F*). Although we were looking for cellular adaptation to ER stress, instead we found that the thyrocytes escaped effects of the drug (Fig. 2*C*) by down-regulating expression of the primary TUN transporter encoded by *Mfsd2a* (Fig. 2*E*) (although these sequential multi-week challenges resulted in thyrocytes with a swollen ER morphology (Fig. 2*D*) looking like that reported in human hypothyroid patients bearing *TG* mutations) (8). To eliminate the ability of thyrocytes to escape the effects of TUN, we resorted to genetic disruption of *Mfsd2a*, and this resulted in cells that were at least an order of magnitude less sensitive to acute TUN exposure before blocking glycosylation of Tg (Fig. 3*C*) and stimulating typical ER stress markers (Fig. 3, *A* and *B*), including stress-mediated ROS generation and cell death (Fig. 3, *D* and *E* and Fig. S2 and Fig. S3). At the same time, *Mfsd2a*-KO cells were normally sensitive to an unrelated acute ER stress agent (thapsigargin, Fig. 3).

In *Mfsd2a*-KO cells treated at the highest dose of TUN (1.5 μg/ml), Tg glycosylation and secretion did not resume (Fig. 4*A* and Fig. S4) and ER stress response continued, including per-

Figure 3. PCCL3 thyrocytes with genetic disruption of *Mfsd2a* are resistant to acute treatment with low-dose TUN but sensitive to high-dose TUN. *A*, *left*, acute TUN dose-response of XBP1 mRNA splicing (*lower band*), an indicator of ER stress response, in control PCCL3 thyrocytes (*upper panel*), or *Mfsd2a*-KO cells (*lower panel*). *Right*, the XBP1 mRNA splicing in *Mfsd2a*-KO cells is not resistant to acute low-dose thapsigargin treatment (*Thaps*, 0.25 μM × 24 h). *B*, acute TUN dose-response of BiP protein, phospho-eIF2a (and total-eIF2a as a loading control), and CHOP—additional indicators of ER stress response—in control PCCL3 thyrocytes (*left*) or *Mfsd2a*-KO cells (*right*), by immunoblotting. *C*, *left*, Tg protein recovered in cells and conditioned (serum-free) media (in a 48-h collection from 24–72 h post treatment) with TUN dose-response in PCCL3 cells (*upper panels*) and *Mfsd2a*-KO cells (*lower panels*); glyco-Tg is the glycosylated form. *D*, acute TUN dose-response of accumulation of ROS (superoxide) in control PCCL3 thyrocytes (*left panel*) and *Mfsd2a*-KO cells after 24 h, was quantified by dihydrorhodamine 123 fluorescence (normalized to total protein), as described previously (37). *E*, cell death measured in PCCL3 and *Mfsd2a*-KO cells at 72 h of TUN treatment.

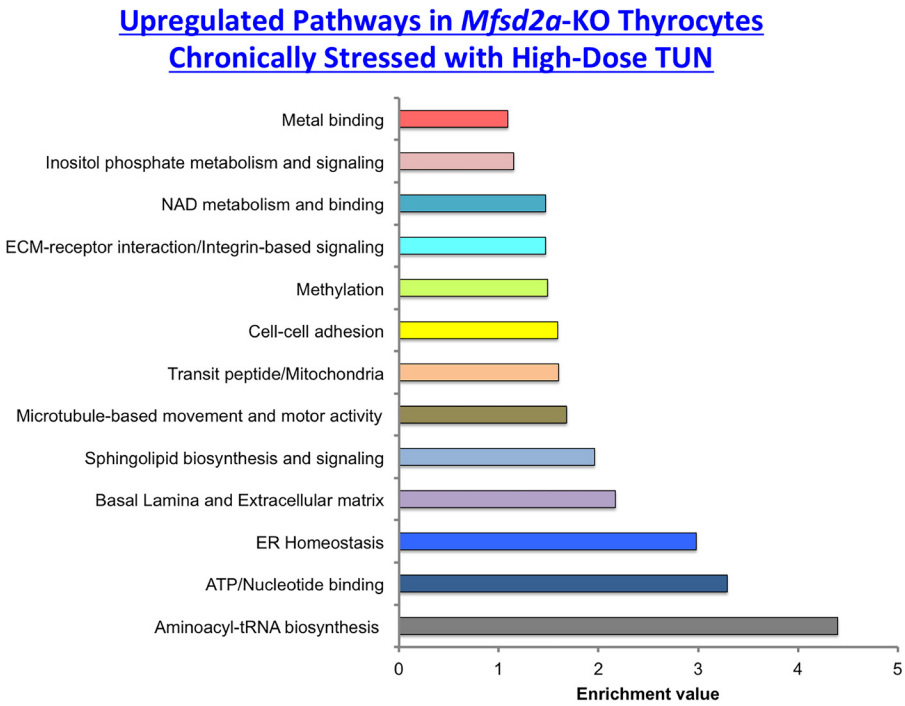

Figure 6. Gene product ontology and functional annotation clustering KEGG and reactome pathways for proteins with up-regulated expression in *Mfsd2a*-KO thyrocytes growing in the chronic continuous presence of high-dose TUN. Proteins showing >20% increase in expression were subjected to DAVID program, KEGG_Pathway and Reactome_pathway analysis. Statistically significant up-regulation of canonical pathways are presented as enrichment values.

sistent phosphorylation of eIF2α (not shown), even after 4 months of continuous culture (Fig. 4, *B* and *C*). Yet, the cells adapted without significant change in their ultimate doubling time. (We also found that chronic TUN-treated *Mfsd2a*-KO cells continued to exhibit a normal acute ER stress response to thapsigargin (data not shown)). Crucially, in this cell culture model, the ambient concentration of TSH, a stimulator of thyrocytes that rises in hypothyroidism (36), was identical between thyrocyte populations grown in the absence or presence of TUN; thus we could ensure that a compensatory TSH increase is not required to achieve comparable growth rates in the chronically stressed thyrocytes.

One of the reproducible responses we observed in the *Mfsd2a*-KO thyrocytes surviving chronic continuous ER stress (from high-dose TUN) with the intracellular accumulation of unglycosylated Tg, was the combination of enhanced phosphorylation that helps to activate AMPK (seen also in the $TG^{cog/cog}$ thyroid *in vivo* (Fig. 5, *A* and *B*) accompanied by decreased phosphorylation of ribosomal S6-kinase and a decrease in overall protein synthesis (Fig. 5, *D* and *E*). Indeed, activation of AMPK also promotes thyrocyte survival to an acute ER stress challenge (Fig. 5*C*). We have recently reported that the combination of up-regulated AMPK activation with down-regulated TOR activation is a cell survival feature in response to ER stress, conserved down to yeast (37). AMPK is an important activator of ER-phagy and mitochondrial function, which is known to be stimulated in ER-stressed cells and can promote disposal of ER protein aggregates (38, 39). Thus perhaps these responses are to be expected, yet to us it is particularly notable that along with decreased levels of phospho–S6-kinase, thyrocytes adapted to chronic continuous ER stress maintain a lower overall protein synthesis level while exhibiting a growth rate that ultimately is comparable to that of unstressed cells. To us, this suggests the likelihood that protein synthesis machinery is less directed to proteins representing thyroid differentiated function (40) while preserving those proteins needed for continued cell growth.

With this in mind, we undertook a comprehensive proteomics analysis of the cells adapted to chronic ER stress. A complete dataset of all proteins analyzed in chronically adapted thyrocytes is found in Table S1. Although some of the most up-regulated proteins are involved in ER homeostasis (Fig. 6), including pathways coupled to ER stress response, (*i.e.* chaperone function, redox homeostasis, and ER lipid biosynthesis), a minority are expected effects attributable to the loss of *N*-glycosylation, such as compensation for diminished cell adherence and extracellular matrix function. However, we did note a decrease in the protein level of several gene products controlling thyroid-differentiated function (Fig. 7*A*). Moreover, we noted a major decrease in the level of *TG* mRNA (confirmed in the thyroids of $TG^{cog/cog}$ mice). These data may be consistent with a re-programming of the translational machinery away from thyrocyte differentiation, and also may potentially be consistent with a decrease in *TG* mRNA stability, analogous to what has been described in several other diseases of secretory protein misfolding (41).

We do not yet fully understand the totality of up-regulated proteins that presumably support survival response in the chronic ER stress-adapted thyrocytes. Indeed, there appear to be additional up-regulated pathways that have yet to be explored by us or others, including iron (metal) metabolism, microtubule binding and motor activity, and methyltransferase

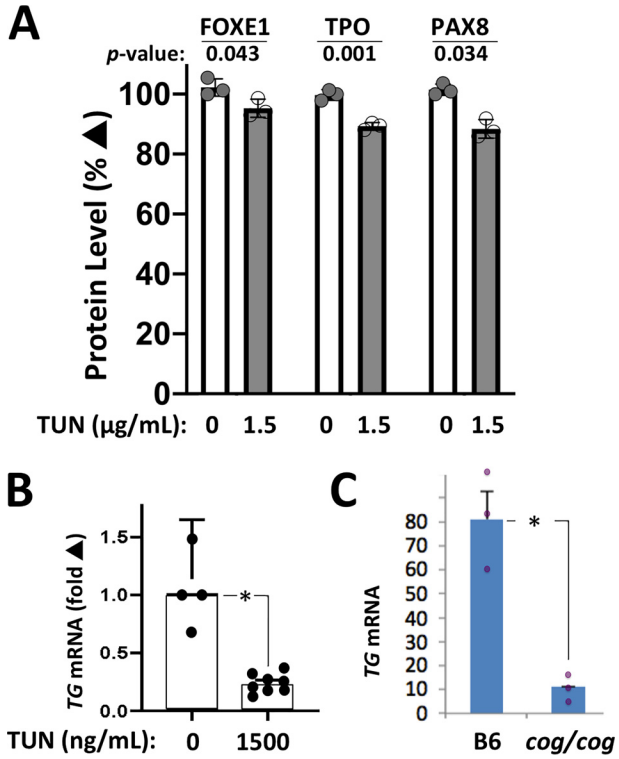

Figure 7. Mfsd2a-KO thyrocytes growing in the chronic continuous presence of high-dose TUN exhibit a decrease in the levels of several proteins representative of the thyroid differentiated phenotype, and decreased *TG* mRNA. *A*, protein levels of FOXE1, TPO, and PAX8 in replicate samples analyzed by LC-MS/MS. Several other proteins representative of thyroid differentiation (TSH receptor, NIS, DUOX2, DUOXA2, Pendrin) were not detected in our proteomics dataset. *B*, *TG* mRNA levels in *Mfsd2a*-KO thyrocytes growing in the chronic continuous presence of high-dose TUN. *C*, *TG* mRNA levels in WT control mouse (C57BL/6, *B6*) and $TG^{cog/cog}$ thyroid tissue, normalized β-actin mRNA (similar results were obtained when normalizing to 18S RNA, not shown).

activity (Fig. 6). Clearly more work is needed to understand the contributions of each of these pathways to the cellular adaptation to chronic ER stress.

Experimental procedures

Materials

Antibodies used were mouse anti-CHOP (Santa Cruz Biotechnology, sc-7351); anti-eIF2α (Santa Cruz Biotechnology, sc-200, sc-11386); rabbit anti-GAPDH and anti–phospho-eIF2α, anti–phospho-AMPK, and anti–phospho–S6-kinase were from Cell Signaling Technology); mouse anti-KDEL (Enzo Life Sciences, ADI-SPA-827); mouse anti-α-tubulin (Sigma-Aldrich, T5168); rat anti-K_i-67 (Dako, M724801-8); and rabbit anti-Tg and anti-BiP as previously described (14). HRP-conjugated secondary antibodies were from Jackson ImmunoResearch Laboratories. Tunicamycin was from Sigma-Aldrich.

Cell lines

PCCL3 cells were maintained in DMEM/F-12 with 5% fetal bovine serum, 1 mIU/ml thyrotropin, 1 μg/ml insulin, 5 μg/ml apo-transferrin, 1 nmol/liter hydrocortisone (the last four from Sigma), and penicillin/streptomycin.

To generate cells with *TG* disruption (KO), 0.8 million PCCL3 cells cultured for 1 d were transfected with 5 μg pX458dg2-r*TG* gRNA plasmid using Lipofectamine 3000. 2 days after transfection, puromycin (0.5 μg/ml) was added $\times$ 2 d; surviving cells were cloned, expanded in complete growth medium, and genotyped to confirm a homozygous 138 – base pair deletion including 65 base pairs of *TG* intron 3 and 73 base pairs of *TG* exon 3, as described previously (42). To generate cells with *Mfsd2a* disruption (KO), 0.8 million PCCL3 cells cultured for 1 d were transfected with 5 μg plasmid bearing gRNA (5′-AATAAGCTTTGCTATGCGGTTGG-3′) using Lipofectamine 3000 and the same procedure (as above) repeated, with genotyping to confirm frameshift *Mfsd2a* mutations in exon 2 (the entire gene contains 14 exons), yielding "clone A2" (with a 4-base insertion) and "clone A5" (with a one-base deletion) and early termination.

Cell death assay

20,000 PCCL3 cells were plated in each well (96-well plates) 24 h before each treatment. Cells were treated as indicated and both dead cells and total cells were measured by the CytoTox-Glo Cytotoxicity Assay Kit (Promega).

Transmission EM

PCCL3 cells were fixed in 1% glutaraldehyde, 1% formaldehyde in 0.1 M Na-cacodylate, pH 7.3. The cells were post fixed in OsO_4, dehydrated, embedded in Epon, and thin sectioned, and grids were examined and micrographs taken on a Philips CM-100 electron microscope.

Cell doubling time

20,000 cells of each cell type were seeded per well at day zero in 24-well plates. At different days after seeding, cells in each well were trypsinized and directly counted (by hemocytometer).

$TG^{cog/cog}$ mice

A breeding pair of $Tgn^{+/cog}$ (C57BL/6) from The Jackson Laboratory were crossbred to generate *cog/cog* mice. Hypothyroid breeders were given supplemental L-thyroxine in drinking water provided *ad libitum* and supplemental L-thyroxine was withdrawn at weaning. Animal use was performed in accordance with the University of Michigan's Committee on Use and Care of Animals.

qRT-PCR

Total RNA was isolated from thyroid tissue or cultured cells using RNeasy Plus (Qiagen) and high-capacity cDNA reverse transcribed (Thermo Fisher Scientific). Real-time PCR was performed using Power SYBR Master Mix or TaqMan Fast Advanced Master Mix on a Step One Plus Real-Time PCR System (Thermo Fisher Scientific). Gene expression was normalized to 18S (cells or tissue) or β-actin (in tissue) (Fig. 7*C*); average CT values were used to calculate relative mRNA expression.

Mass spectrometry

Cells were scraped and homogenized in 40 mM TEAB buffer containing 5 mM DTT 2% LiDS. After 10 min at room temperature, reduced samples were alkylated with iodoacetimide (15

mM final) for 1 h at room temperature, followed by quenching with an additional 10 mM DTT. Samples were de-salted in Pierce Handee spin columns and aliquots of 50 μg protein from each sample were diluted in 40 mM TEAB buffer and precipitated with 2 volumes 100% methanol plus 1 mM acetic acid for 1 h at room temperature. The precipitates were dried and then solubilized by sonication in 0.3% deoxycholate, 40 mM TEAB, and 1× PBS, followed by an overnight digestion with sequencing-grade trypsin (Promega). A 20-μg aliquot of each digest was then labeled with Tandem Mass Tag labeling reagents (Thermo Scientific) as per the manufacturer's instructions. The labeled peptides were pooled and fractionated using the Pierce High pH Reversed-Phase Peptide Fractionation Kit and separated by reversed-phase chromatography using a PepMap100 C18 column (Thermo Scientific) followed by ionization with the Easy Spray Ion Source (Thermo Scientific) and finally introduced into a Fusion mass spectrometer (Thermo Scientific). 2-hour chromatography gradients were used. MS1 scans were collected at 120,000 resolution and MS2 scans at 50,000. Data-dependent MS2 scans of abundant species were collected for 5 s per cycle using high-energy collision dissociation at 40% collision energy.

Bioinformatics

Raw files were searched using Thermo Proteome Discoverer version 2.1.1.21 using the Sequest HT node for the sequence database search. Peptide sequences were from the UniProt Rat Proteome downloaded 2018–12-21 (21,898 sequences) requiring tryptic peptides at least six residues long with at most two missed cleavage sites. Precursor mass tolerance was 20 ppm and fragment tolerance was 0.02 Da. Methionine oxidation and protein N-terminal acetylation were variable modifications and TMT labels and cysteine carbamidomethylation were fixed modifications. Peptide identifications were accepted at a 1% false discovery rate as determined by a reversed database. This corresponds to a percolator PEP of 0.28.

Statistical analysis was done in R v3.6.2. Channels were normalized to all have the same median abundance and log2 transformed. Differences between treatment groups were identified using a moderated *t* test (43) with q-value multiple test correction (44). Proteins with significant change in abundance based on MS data and *t* test were selected (significance threshold for expression change was 20%) and subjected to annotation and pathway analysis using the DAVID program, KEGG-Pathway, and Reactome pathway analysis (the algorithms in this case use only the proteins in the list, regardless of protein expression values). The *p* value and the Benjamini-Hochberg false discovery rate were used to determine significance of enrichment. The canonical pathways were scored based on *p* values. Pathways with most significant changes are presented.

Western blotting

Thyroid was disrupted in 50 mM Hepes, pH 7.4, 150 mM NaCl, 0.1% SDS, 1% Nonidet P-40, 2 mM EDTA, protease inhibitor mixture (Roche); cultured cells were lysed in RIPA buffer with protease and phosphatase inhibitor (Pierce Biotechnologies). Total protein was measured by BCA assay (Pierce Biotechnologies). Samples resolved by SDS-PAGE were electrotransferred to nitrocellulose and immunoblotted using antibodies as described in the figure legends, and detected by SuperSignal West Pico Chemiluminescent Substrate (Pierce Biotechnologies).

Immunofluorescence and immunohistochemistry

Cultured thyrocytes were fixed with 4% formaldehyde, washed twice with PBS, permeabilized with 0.4% Triton X-100 in TBS for 20 min (room temperature) and blocked with 3% BSA in 0.2% Triton X-100 in TBS for 1 h (room temperature). For thyroid tissue, 5-μm sections of fixed, paraffin-embedded tissue were deparaffinzed in Citrisolv, rehydrated in a graded series of alcohols, with antigen unmasking in Retrieve-All (Covance) at 90 °C for 2 h. After cooling and washing, sections were blocked for 1 h with 0.3% Triton-X, 10% normal goat serum in PBS. The cultured cells were incubated overnight at 4 °C with indicated primary antibodies, and then with secondary antibodies conjugated to Alexa Fluor 488 or Alexa Fluor 555 (Thermo-Fisher). Slides were washed and coverslips mounted with Prolong Gold with DAPI (Thermo-Fisher), with images captured on an Olympus FV500 confocal microscope. For K_i-67 immunohistochemistry using the ABC staining kit (Vector Labs), after antigen retrieval, slides were pretreated with 3% H_2O_2, incubated with blocking solution, and then incubated anti K_i-67 for 30 min with biotinylated secondary antibody followed by incubation with avidin-HRP, and finally with DAB (room temperature). Sections were incubated for 30 min (room temperature) to visualize reaction product. Tissue was counterstained with hematoxylin. Images were captured on a Nikon E800 microscope.

Statistics and microarray

For experiments conducted in PCCL3 cells, one-sided analysis of variance with Tukey's post hoc test was performed. Data are represented as mean ± S.D. unless otherwise noted, with $p \leq 0.05$ determined to be significant.

Data availability

1) Increased phospho-eIF2α in *Mfsd2a*-KO thyrocytes grown in the continuous presence of 1500 ng/ml TUN; 2) chronic TUN-treated *Mfsd2a*-KO cells exhibiting a normal acute ER stress response to thapsigargin; and 3) for Fig. 7*C*, *TG* mRNA levels in WT control and $TG^{cog/cog}$ mouse thyroid tissue normalized to 18S RNA are all data available upon request (Dr. Peter Arvan, University of Michigan, E-mail: parvan@umich.edu). All other data are contained within the manuscript. The raw mass spectrometry is publicly and permanently accessible from MassIVE repository with the dataset identifier MSV000085006 and ProteomeXchange (PXD017724).

Author contributions—Y. M., O. K., and P. A. data curation; Y. M., O. K., and P. A. formal analysis; Y. M., O. K., and A. P. K. validation; Y. M., O. K., K. Z. Y., A. P. K., and A. C. investigation; Y. M., O. K., K. Z. Y., A. P. K., and A. C. methodology; Y. M., O. K., A. P. K., A. C., and P. A. writing-original draft; Y. M., O. K., K. Z. Y., A. P. K., A. C., and P. A. writing-review and editing; A. C. and P. A. conceptualization; A. C. and P. A. supervision; A. C. and P. A. funding acquisition.

Acknowledgments—We thank Dennis Larkin, Hao Zhang, and Jeffrey Knupp (University of Michigan) for assistance in multiple aspects of this work.

References

1. Han, J., and Kaufman, R. J. (2017) Physiological/pathological ramifications of transcription factors in the unfolded protein response. *Genes Dev.* **31,** 1417–1438 CrossRef Medline
2. Tsang, K. Y., Chan, D., Bateman, J. F., and Cheah, K. S. (2010) In vivo cellular adaptation to ER stress: Survival strategies with double-edged consequences. *J. Cell Sci.* **123,** 2145–2154 CrossRef Medline
3. Ghosh, R., Colon-Negron, K., and Papa, F. R. (2019) Endoplasmic reticulum stress, degeneration of pancreatic islet β-cells, and therapeutic modulation of the unfolded protein response in diabetes. *Mol. Metab.* **27,** (suppl.) S60–S68 CrossRef Medline
4. Szabat, M., Page, M. M., Panzhinskiy, E., Skovsø, S., Mojibian, M., Fernandez-Tajes, J., Bruin, J. E., Bround, M. J., Lee, J. T., Xu, E. E., Taghizadeh, F., O'Dwyer, S., van de Bunt, M., Moon, K. M., Sinha, S., *et al.* (2016) Reduced insulin production relieves endoplasmic reticulum stress and induces β cell proliferation. *Cell Metab.* **23,** 179–193 CrossRef Medline
5. Oakes, S. A., and Papa, F. R. (2015) The role of endoplasmic reticulum stress in human pathology. *Annu. Rev. Pathol.* **10,** 173–194 CrossRef Medline
6. Targovnik, H. M., Scheps, K. G., and Rivolta, C. M. (2020) Defects in protein folding in congenital hypothyroidism. *Mol. Cell Endocrinol.* **501,** 110638 CrossRef Medline
7. Ryoo, H. D. (2016) Long and short (timeframe) of endoplasmic reticulum stress-induced cell death. *FEBS J.* **283,** 3718–3722 CrossRef Medline
8. Medeiros-Neto, G., Kim, P. S., Yoo, S. E., Vono, J., Targovnik, H. M., Camargo, R., Hossain, S. A., and Arvan, P. (1996) Congenital hypothyroid goiter with deficient thyroglobulin. Identification of an endoplasmic reticulum storage disease (ERSD) with induction of molecular chaperones. *J. Clin. Invest.* **98,** 2838–2844 CrossRef Medline
9. Di Jeso, B., and Arvan, P. (2016) Thyroglobulin from molecular and cellular biology to clinical endocrinology. *Endocr. Rev.* **37,** 2–36 CrossRef Medline
10. Citterio, C. E., Targovnik, H. M., and Arvan, P. (2019) The role of thyroglobulin in thyroid hormonogenesis. *Nat. Rev. Endocrinol.* **15,** 323–338 CrossRef Medline
11. Tabas, I., and Ron, D. (2011) Integrating the mechanisms of apoptosis induced by endoplasmic reticulum stress. *Nat. Cell Biol.* **13,** 184–190 CrossRef Medline
12. Medeiros-Neto, G., Targovnik, H. M., and Vassart, G. (1993) Defective thyroglobulin synthesis and secretion causing goiter and hypothyroidism. *Endocr. Rev.* **14,** 165–183 CrossRef Medline
13. Kim, P. S., Hossain, S. A., Park, Y. N., Lee, I., Yoo, S. E., and Arvan, P. (1998) A single amino acid change in the acetylcholinesterase-like domain of thyroglobulin causes congenital goiter with hypothyroidism in the cog/cog mouse: A model of human endoplasmic reticulum storage diseases. *Proc. Natl. Acad. Sci. U.S.A.* **95,** 9909–9913 CrossRef Medline
14. Kim, P. S., Kwon, O.-Y., and Arvan, P. (1996) An endoplasmic reticulum storage disease causing congenital goiter with hypothyroidism. *J. Cell Biol.* **133,** 517–527 CrossRef Medline
15. Di Jeso, B., Ulianich, L., Pacifico, F., Leonardi, A., Vito, P., Consiglio, E., Formisano, S., and Arvan, P. (2003) The folding of thyroglobulin in the calnexin/calreticulin pathway and its alteration by a loss of Ca2+ from the endoplasmic reticulum. *Biochem. J.* **370,** 449–458 CrossRef Medline
16. Van Herle, A. J., Vassart, G., and Dumont, J. E. (1979) Control of thyroglobulin synthesis and secretion. Part one. *N. Eng. J. Med.* **301,** 239–249 CrossRef Medline
17. Reiling, J. H., Clish, C. B., Carette, J. E., Varadarajan, M., Brummelkamp, T. R., and Sabatini, D. M. (2011) A haploid genetic screen identifies the major facilitator domain containing 2A (MFSD2A) transporter as a key mediator in the response to tunicamycin. *Proc. Natl. Acad. Sci. U.S.A.* **108,** 11756–11765 CrossRef Medline
18. Moritake, H., Obara, M., Saito, Y., Kashimada, A., Takagi, M., Funakoshi-Tago, M., Fukuyama, T., Yoshioka, M., Inoue, A., Komatsu, H., Nishitoh, H., Kataoka, H., and Nunoi, H. (2017) A mouse model reveals that Mfsd2a is critical for unfolded protein response upon exposure to tunicamycin. *Hum. Cell* **30,** 88–97 CrossRef Medline
19. Yoshida, H., Matsui, T., Yamamoto, A., Okada, T., and Mori, K. (2001) XBP1 mRNA is induced by ATF6 and spliced by IRE1 in response to ER stress to produce a highly active transcription factor. *Cell* **107,** 881–891 CrossRef Medline
20. Harding, H. P., Zhang, Y., and Ron, D. (1999) Protein translation and folding are coupled by an endoplasmic-reticulum-resident kinase. *Nature* **397,** 271–274 CrossRef Medline
21. Harding, H. P., Novoa, I., Zhang, Y., Zeng, H., Wek, R., Schapira, M., and Ron, D. (2000) Regulated translation initiation controls stress-induced gene expression in mammalian cells. *Mol. Cell* **6,** 1099–1108 CrossRef Medline
22. Adkison, L. R., Taylor, S., and Beamer, W. G. (1990) Mutant gene-induced disorders of structure, function and thyroglobulin synthesis in congenital goitre (*cog*/*cog*) in mice. *J. Endocrinol.* **126,** 51–58 CrossRef Medline
23. Hay, N., and Sonenberg, N. (2004) Upstream and downstream of mTOR. *Genes Dev.* **18,** 1926–1945 CrossRef Medline
24. Tanjore, H., Cheng, D. S., Degryse, A. L., Zoz, D. F., Abdolrasulnia, R., Lawson, W. E., and Blackwell, T. S. (2011) Alveolar epithelial cells undergo epithelial-to-mesenchymal transition in response to endoplasmic reticulum stress. *J. Biol. Chem.* **286,** 30972–30980 CrossRef Medline
25. Shimura, H., Suzuki, H., Miyazaki, A., Furuya, F., Ohta, K., Haraguchi, K., Endo, T., and Onaya, T. (2001) Transcriptional activation of the thyroglobulin promoter directing suicide gene expression by thyroid transcription factor-1 in thyroid cancer cells. *Cancer Res.* **61,** 3640–3646 Medline
26. Maurel, M., Chevet, E., Tavernier, J., and Gerlo, S. (2014) Getting RIDD of RNA: IRE1 in cell fate regulation. *Trends Biochem. Sci.* **39,** 245–254 CrossRef Medline
27. Kim, P. S., and Arvan, P. (1998) Endocrinopathies in the family of endoplasmic reticulum (ER) storage diseases: Disorders of protein trafficking and the role of ER molecular chaperones. *Endocr. Rev.* **19,** 173–202 CrossRef Medline
28. Fregonese, L., and Stolk, J. (2008) Hereditary alpha-1-antitrypsin deficiency and its clinical consequences. *Orphanet J. Rare Dis.* **3,** 16 CrossRef Medline
29. Wu, J., Rutkowski, D. T., Dubois, M., Swathirajan, J., Saunders, T., Wang, J., Song, B., Yau, G. D., and Kaufman, R. J. (2007) ATF6α optimizes long-term endoplasmic reticulum function to protect cells from chronic stress. *Dev. Cell* **13,** 351–364 CrossRef Medline
30. Sharma, R. B., O'Donnell, A. C., Stamateris, R. E., Ha, B., McCloskey, K. M., Reynolds, P. R., Arvan, P., and Alonso, L. C. (2015) Insulin demand regulates β cell number via the unfolded protein response. *J. Clin. Invest.* **125,** 3831–3846 CrossRef Medline
31. Riahi, Y., Israeli, T., Yeroslaviz, R., Chimenez, S., Avrahami, D., Stolovich-Rain, M., Alter, I., Sebag, M., Polin, N., Bernal-Mizrachi, E., Dor, Y., Cerasi, E., and Leibowitz, G. (2018) Inhibition of mTORC1 by ER stress impairs neonatal β-cell expansion and predisposes to diabetes in the *Akita* mouse. *Elife* **7,** e38472 CrossRef Medline
32. Balboa, D., Saarimaki-Vire, J., Borshagovski, D., Survila, M., Lindholm, P., Galli, E., Eurola, S., Ustinov, J., Grym, H., Huopio, H., Partanen, J., Wartiovaara, K., and Otonkoski, T. (2018) Insulin mutations impair β-cell development in a patient-derived iPSC model of neonatal diabetes. *Elife* **7,** e38519 CrossRef Medline
33. Han, J., Back, S. H., Hur, J., Lin, Y. H., Gildersleeve, R., Shan, J., Yuan, C. L., Krokowski, D., Wang, S., Hatzoglou, M., Kilberg, M. S., Sartor, M. A., and Kaufman, R. J. (2013) ER-stress-induced transcriptional regulation increases protein synthesis leading to cell death. *Nat. Cell Biol.* **15,** 481–490 CrossRef Medline
34. Sano, R., and Reed, J. C. (2013) ER stress-induced cell death mechanisms. *Biochim. Biophys. Acta* **1833,** 3460–3470 CrossRef Medline
35. Hishinuma, A. (2005) Thyroglobulin gene abnormalities (in Japanese). *Rinsho Byori.* **53,** 935–941 Medline

36. Peters, C., van Trotsenburg, A. S. P., and Schoenmakers, N. (2018) Diagnosis of endocrine disease. Congenital hypothyroidism: Update and perspectives. *Eur. J. Endocrinol.* **179,** R297–R317 CrossRef Medline
37. Knupp, J., Arvan, P., and Chang, A. (2019) Increased mitochondrial respiration promotes survival from endoplasmic reticulum stress. *Cell Death Differ.* **26,** 487–501 CrossRef Medline
38. Cunningham, C. N., Williams, J. M., Knupp, J., Arunagiri, A., Arvan, P., and Tsai, B. (2019) Cells deploy a two-pronged strategy to rectify misfolded proinsulin aggregates. *Mol. Cell* **75,** 442–456.e4 CrossRef Medline
39. Herzig, S., and Shaw, R. J. (2018) AMPK: Guardian of metabolism and mitochondrial homeostasis. *Nat. Rev. Mol. Cell Biol.* **19,** 121–135 CrossRef Medline
40. Wen, G., Ringseis, R., and Eder, K. (2017) Endoplasmic reticulum stress inhibits expression of genes involved in thyroid hormone synthesis and their key transcriptional regulators in FRTL-5 thyrocytes. *PLoS One* **12,** e0187561 CrossRef Medline
41. Morishita, Y., and Arvan, P. (2020) Lessons from animal models of endocrine disorders caused by defects of protein folding in the secretory pathway. *Mol. Cell Endocrinol.* **499,** 110613 CrossRef Medline
42. Citterio, C. E., Morishita, Y., Dakka, N., Veluswamy, B., and Arvan, P. (2018) Relationship between the dimerization of thyroglobulin and its ability to form triiodothyronine. *J. Biol. Chem.* **293,** 4860–4869 CrossRef Medline
43. Smyth, G. K. (2004) Linear models and empirical Bayes methods for assessing differential expression in microarray experiments. *Stat. Appl. Genet. Mol. Biol.* **3,** 1–25 CrossRef Medline
44. Storey, J. D., and Tibshirani, R. (2003) Statistical significance for genome-wide studies. *Proc. Natl. Acad. Sci. U.S.A.* **100,** 9440–9445 CrossRef Medline